Characterization of Electrodeposited Gold and Palladium Nanowire Gratings with Optical Diffraction Measurements

Aaron R. Halpern, **Naoya Nishi**, **Jia Wen**, **Fan Yang**, **Chengxiang Xiang**, **Reginald M. Penner**, and **Robert M. Corn**[*]
Department of Chemistry, University of California-Irvine, Irvine, CA 92697, USA

Abstract

Parallel arrays of either Au or Pd nanowires were fabricated on glass substrates via the electrochemical process of lithographically patterned nanowire electrodeposition (LPNE) and then characterized with scanning electron microscopy (SEM) and a series of optical diffraction measurements at 633 nm. Nanowires with widths varying from 25 nm to 150 nm were electrodeposited onto nanoscale Ni surfaces created by the undercut etching of a photoresist pattern on a planar substrate. Using a simple transmission grating geometry, up to 60 diffraction orders were observed from the nanowire gratings, with separate oscillatory intensity patterns appearing in the even and odd diffraction orders. The presence of these intensity oscillations is attributed to LPNE array fabrication process, which creates arrays with alternating interwire spacings of distances $d+\Delta$ and $d-\Delta$, where $d = 25$ μm and the asymmetry Δ varied from 0 to 3.5 μm. The amount of asymmetry could be controlled by varying the LPNE undercut etching time during the creation of the nanoscale Ni surfaces. The Fourier transform of a mathematical model of the nanowire array was used to predict the diffraction intensity patterns and quantitatively determine Δ for any grating. Additional sensitivity and an expanded diffraction order range were obtained through the use of external reflection (ER) and total internal reflection (TIR) diffraction geometries.

Nanowires are a promising class of nanometer-sized structures with useful electrical, optical, and mechanical properties that vary significantly from those of the bulk material.[1-3] For example, when used as a sensor material, the high surface-to-volume ratio of nanowires makes them extremely responsive to gases,[4-7] and to chemical and biological species.[8-10] The specific methodology employed in the fabrication of a nanowire will strongly affect its local atomic structure and shape; these nanoscale features will in turn determine its unique physical properties. For example, metal nanowires formed by the process of electrochemical deposition have a unique crystallinity, mechanical structure and electrical conductivity.[3, 11]

In addition to the morphology of the nanowire on the nanometer scale, it is also important to be able to create assemblies and ordered arrays of nanowires at specific desired positions and orientations on supporting substrates for the successful application of these nanomaterials in useful devices. Penner and coworkers have developed a novel fabrication methodology for creating micron-scaled nanowire patterns on surfaces.[12] This process is denoted as lithographically patterned nanowire electrodeposition (LPNE), and combines top-down lithographic photopatterning with nanoscale electrodeposition methods to create structures such as arrays of hundreds of parallel nanowires on surfaces, micron-sized squares and circles of nanowires, and more complex patterns on the micron and millimeter length scales. The width and height of the nanowires created in LPNE process can be controlled with a resolution of 5 nm.[13]

*rcorn@uci.edu.

Visible light diffraction is a simple and inexpensive optical method that is highly sensitive to the structure of the light scattering medium and has been studied for high-sensitivity chemical and biochemical sensing.[14-25] For example, diffraction-based bioaffinity sensors has been used to detect DNA,[19, 22, 24, 25] proteins,[14, 20-23] and cells.[15, 17] One advantage of diffraction-based bioaffinity sensors is that they discriminate against nonspecific adsorption processes to the entire substrate because only patterned bioaffinity adsorption will lead to changes in the diffraction signal. This has been seen before in both metal and dielectric gratings.[14, 15, 17, 19-25]

In this paper, we are particularly interested in the fabrication of nanowire arrays or gratings with potential applications to diffraction-based chemical and biochemical sensing. Specifically, we have characterized the diffraction properties of gold and palladium nanowire arrays created on BK-7 glass substrates via the LPNE process. Diffraction spots are easily observed from the nanowire gratings, even though the nanowires can cover less than 0.1% of the surface. Scanning electron microscopy (SEM) measurements are used to verify the local structure of the nanowire arrays. Techniques such as SEM, transmission electron microscopy (TEM), and scanning probe microscopy (SPM) can provide beautiful nanoscale images of metal nanowires; however, these methods can be difficult to implement on larger length scales (e.g., centimeters), and cannot follow rapidly evolving changes in surface structure as well as optical methods such as diffraction.

The optical diffraction properties are directly related to the physical structure of these nanowire gratings. We will eventually be interested in using these optical diffraction methods for chemical sensing, but in this paper we lay the groundwork for those future measurements by carefully analyzing the unusual diffraction patterns that are observed from these nanowire arrays. The diffraction patterns are very different from those obtained from typical micron-sized gratings; we quantitatively show how small asymmetries in the nanowire gratings that are created during the LPNE fabrication process significantly affect the nanowire diffraction patterns.

Experimental Section

Grating Fabrication

Nanowire gratings were fabricated on BK-7 glass substrates (Schott Glass) using the LPNE technique.[12, 13] The gratings were either Au or Pd with widths of 25−150 nm and average inter-nanowire spacing of 25 μm.

SEM Measurements

SEM images were taken on a Zeiss Ultra 55 at 5 keV. Prior to imaging, samples were sputter coated with a 1−2 nm Au film to prevent charging.

Diffraction Measurements

Diffraction intensities were obtained using a HeNe Laser (LHRP-1201, Research Electro-Optics, 633 nm, 12 mW). A combination of a Glan-Thompson polarizer (Newport) and a λ/2 plate (Special Optics) was used to vary the laser power. The diffraction pattern was focused onto high quality printer paper (Premium Plus High Gloss, HP) with a 9" FL lens (Newport) and imaged from a distance with a scientific monochrome CCD camera (QIC-F-M-12, 1392 × 1064 pixels, QImaging) with a 55mm TV lens. The paper screen was automatically raised at ~20 μm/s, while 300 images were taken. The images were averaged to remove "hot spots" on the paper surface. In TIR geometry, a BK-7 prism was coupled to the nanowire grating substrate with η = 1.5160 index matching oil. Exact scattering geometries are described in Results and Discussion.

Diffraction Spot Intensity Analysis

A "line profile" was generated by vertically averaging twenty pixel rows containing the diffraction pattern. Twenty rows above and below were also averaged, then subtracted off as a baseline. Each diffraction peak was contained by at least fifteen data points and was individually fit with a Gaussian to find its position with respect to the main beam and integrated to obtain its intensity.

Results and Discussion

Fabrication of Gold and Palladium Nanowire Arrays

Periodic arrays of either Au or Pd nanowires spaced by approximately 25 μm were created on BK-7 glass substrates by the LPNE process as shown in Figure 1. Briefly, a 45 nm Ni layer was first vapor deposited onto a glass slide and then coated with a positive photoresist. The photoresist was patterned into stripes of width d = 25 μm that were separated by 25 μm of exposed Ni using standard photopatterning techniques (Step A in Figure 1). The exposed Ni areas were then etched away with a dilute nitric acid solution (Step B). The etching process also created a "trench" under each of the photoresist edges with a height h of 45 nm and a depth E which varied with etching time from 100 to 2000 nm. Either Au or Pd was then electrochemically deposited onto the exposed Ni in the trench to form continuous nanowires of width w which varied from 25 to 150 nm as determined by the deposition time (Step C). Finally, the remaining photoresist and Ni were removed to create arrays of up to 700 nanowires with lengths up to 1 cm on the glass substrate (Step D).

As shown in Figure 1, the etching process imparts an asymmetry to the array, so that the spacing between nanowires alternates between $d+\Delta$ and $d-\Delta$ where the asymmetry Δ is given by eq 1:

$$\Delta = 2E - w \tag{1}$$

A series of SEM experiments were used to characterize the average spacing, asymmetry and width of the Au and Pd nanowire arrays. Figure 2a shows a typical large area SEM image of Au nanowires with an average spacing of 25 μm. A closer analysis (Figure 2b) of the figure reveals the alternate spacing predicted by the LPNE process in Figure 1 with an asymmetry Δ of 0.9 μm for this particular nanowire array. The size of the asymmetry varied from array to array, and depended on both the trench depth E and the nanowire width w as given by eq 1. A higher magnification SEM image (Figure 2c) showed an average width of 120 nm for a single Au nanowire in this particular array. TEM images also revealed the nanoscale structure of the electrodeposited Au nanowires; this nanowire grain structure has been discussed previously.[3]

Nanowire Array Diffraction Measurements in Transmission Geometry

Diffraction experiments were performed on these nanowire arrays using a 633 nm HeNe laser focused to a 0.5 mm beam width (which illuminated approximately 20 nanowires) in three different experimental geometries shown schematically in Figure 3: transmission (Figure 3a), external reflection (ER) (Figure 3b), and total internal reflection (TIR) (Figure 3c). An image of the diffraction pattern was captured with a CCD camera as described in Experimental Section. In this section, diffraction measurements obtained in the transmission geometry are discussed. Diffraction measurements obtained using ER and TIR geometries are discussed in a subsequent section.

Typical diffraction data obtained in the transmission geometry from a 120 nm Au nanowire array are shown in Figure 4. The bottom of the figure shows an enhanced contrast image of the diffraction spots obtained from the array. Plotted in the figure is a "line profile" of the diffraction image that was generated by binning columns of CCD pixels. Three striking features

are immediately evident from this line profile: (i) the nanowire arrays display many orders of diffraction (typically up to 60), (ii) the intensities of the even and odd orders are both modulated with a periodicity of approximately 20 orders, and (iii) the modulation of the even and odd orders appears to be out of phase with each other. Each of these features is a direct result of the structure of the nanowire arrays generated by the LPNE process, and can be analyzed quantitatively.

Measurements of the positions of the diffraction spots in the line profile in Figure 4 were used to determine the diffraction order numbers and grating periodicity. As shown in Figure 5, diffraction from the nanowire array in transmission geometry was found to obey the simple grating equation (eq 2):

$$m\lambda = D\sin\theta_m \tag{2}$$

where m is the diffraction order $(0, \pm 1, \pm 2...)$, λ is the wavelength, D is the grating period, and θ_m is the angle of the diffracted ray from the normal as defined in Figure 5. An order number m was assigned to each diffraction spot by counting from the $m = 0$ position on the screen, and a value of $\sin\theta_m$ was determined for each diffraction spot from the function $x_M/(x_m^2 + L^2)^{1/2}$ where x_m was the distance of that diffraction peak in the image from the $m = 0$ position and L was the distance between the screen and the sample (see the lower inset in Figure 5). The solid circles in the Figure are the experimentally determined $(\sin\theta_m, m)$ pairs, and the solid line is a fit of the data to eq 2.

As evident from eq 2, the slope of the line in Figure 5 has a value of D/λ; from this slope a value of D was repeatedly observed to be 50.2 ± 0.1 μm for all of the nanowire arrays. This value of D is twice the average spacing between nanowires (25 μm), and is a direct consequence of the asymmetry of the nanowire array. As shown in the top inset of Figure 5, the full periodicity of the array is $D = (d-\Delta) + (d+\Delta) = 2d = 50$ μm.

If the asymmetry Δ were zero, then the grating period would have been not 50 μm, but 25 μm. The distance between the diffraction spots in the image would have been doubled; in other words, all of the odd order peaks would have disappeared. Thus, we see that the only reason that the diffraction exhibits this unique even order/odd order alternating intensity pattern is due to the asymmetry introduced into the nanowire array due to the LPNE fabrication process.

To further analyze the even order/odd order alternating intensity patterns, the peaks in the transmission diffraction line profile in Figure 4 are integrated and re-plotted as a function of m in Figure 6 (details of the image analysis are given in Experimental Section). Integration of the diffraction peaks is necessary since the widths of the transmission diffraction peaks become larger at high order number due to the increase in the angle θ_m. In Figure 6 we see that the even order and odd order peaks both exhibit oscillating intensity patterns that are not in phase with each other. Also labeled in the Figure are the orders where the oscillating intensity patterns have a minimum for both the even and odd order diffraction intensities. The first minimum in the even order peaks occurs at order $m = 26$; this order is denoted as "E_1". The first minimum in the odd order peaks occurs at order $m = 51$ and this order is denoted as "O_1". The order numbers for the additional minima are defined as E_2, O_2 etc. The pattern of order numbers E_n and O_n will be used in the next section to determine the asymmetry Δ.

Asymmetry Determination of LPNE Nanowire Arrays

The oscillating intensity patterns observed in the even and odd order diffraction peaks from the nanowire arrays produced by the LPNE process can be used to determine the asymmetry Δ for any given array. A simple method for this asymmetry determination is to first measure

the sets of order numbers E_n and O_n at which minima in the even and odd order diffraction intensities are observed. Then these two sets of order numbers are compared with theoretical values based on the magnitude of the asymmetry Δ. For this theoretical calculation, we model the diffraction patterns from the nanowire arrays in the Fraunhofer (far-field) region by taking the Fourier Transform (FT) of a numerical model[17, 20, 26] of the array created from the convolution of an asymmetric grating unit cell with a Dirac comb. The FT is obtained directly in Fourier space from the product of the FT of the unit cell with the FT of the Dirac comb. In this section, we briefly describe how the FT is obtained, and then how theoretical values of order numbers E_n and O_n are extracted and then used to determine a value of Δ from the diffraction data. The complete mathematical details of this theoretical calculation are given in Appendix.

To model the nanowire array, an asymmetric grating unit cell was created that was then convoluted with a Dirac comb. The asymmetric grating unit cell consisted of two square pulses centered at zero and at $d-\Delta$ both of width w and amplitude A as shown schematically in Figure 7a. The amplitude A contains several factors including thickness of the nanowires and the refractive index difference between the metal and media. If this unit cell is convoluted with a Dirac comb consisting of an infinite array of delta functions with spacing $2d$ (Figure 7b), the result is an asymmetric infinite array of square pulses of width w with alternating spacing of $d-\Delta$ and $d+\Delta$ (Figure 7c). The function shown schematically in Figure 7c serves as a model for the nanowire array; the FT of this function will yield a theoretical model of the diffraction pattern.

The FT of the asymmetric infinite array is not taken directly; instead, using the convolution theorem we find the FT in the Fourier domain. We first need the FT of the asymmetric unit cell (plotted as the square magnitude in Figure 7d) and the FT of the Dirac comb (a new Dirac comb with spacing $1/2d$ as displayed in Figure 7e). These two FTs are then multiplied together to obtain the FT of the asymmetric infinite array. Since we are concerned with the integrated intensity of the diffraction peaks, we integrate the FT over an infinitesimal interval around each order, essentially "sampling" the FT of the unit cell at integer multiples of $1/2d$ and finally take the magnitude squared (Figure 7f). Each sample point represented by a solid blue (even) or open red (odd) dot is one order of the diffraction pattern. Notice that the intensity oscillations of the even and odd orders in Figure 7f arise naturally from this sampling process.

The analytical functions can be obtained which describe the oscillatory patterns of the sampled intensities of the even and odd orders in Figure 7f (the blue and red solid lines). The complete details of this calculation are in Appendix; the results are given in eqs 3 and 4:

$$I_e(m) = \frac{A^2 w^2}{d^2} \cos^2\left(\frac{\pi}{2}\frac{\Delta}{d}m\right) \operatorname{sinc}^2\left(\frac{\pi}{2}\frac{w}{d}m\right) \qquad (m \quad \text{even})$$

(3)

$$I_o(m) = \frac{A^2 w^2}{d^2} \sin^2\left(\frac{\pi}{2}\frac{\Delta}{d}m\right) \operatorname{sinc}^2\left(\frac{\pi}{2}\frac{w}{d}m\right) \qquad (m \quad \text{odd})$$

(4)

where $I_e(m)$ and $I_o(m)$ are the two intensity functions for even and odd diffraction orders (m) respectively. Notice that the intensity functions depend on the square of the width of the nanowires w and the decay of the sinc^2 function. The periodicity of the sinc^2 function is proportional to the ratio of the nanowire width to the average spacing between nanowires in the array (w/d). Because $w \ll d$, the sinc^2 function decreases very slowly. This slow decrease is the reason why so many (> 60) orders are observed in the nanowire diffraction pattern of the

present study. This is not the case in usual micron-sized gratings or even in nanowire arrays with submicron-scale spacing.[27]

The $\cos^2$ and $\sin^2$ terms in eqs 3 and 4 respectively can be used to determine the asymmetry since they only depend on the ratio Δ/d. These two terms oscillate at a faster frequency than the sinc^2 function, even for small values of Δ. The $\cos^2$ and $\sin^2$ terms are responsible for the minima E_n and O_n respectively that we observe in the diffraction data (*e.g.*, E_1 and O_1 in Figure 6). As shown in Appendix, the orders at which these minima occur are defined as a two sets of order numbers, E_n and O_n, given by eqs 5 and 6:

$$E_n = \frac{d}{\Delta}(2n-1) \qquad\qquad (n=1,2,3\ldots)$$

(5)

$$O_n = \frac{d}{\Delta}2n \qquad\qquad (n=1,2,3\ldots)$$

(6)

Both of these sets depend upon the inverse of the asymmetry ratio Δ/d. Figure 8 plots the minimum orders E_n (solid lines) and O_n (dotted lines) that would be observed from order number 0 to 60 as a function of the percent asymmetry ratio ($\%\Delta/d$) from 0 to 14%. This plot can be used to determine the asymmetry of a given nanowire array from its diffraction data. For example, the data in Figure 6 exhibit two minima, E_1 and O_1, at orders 24 and 51 respectively. These two values are plotted as the open-crossed symbols in Figure 8. From the plot, it can be seen that only one asymmetry ratio, 4.0%, matches these two observed order numbers with theoretical values of E_1 and O_1. Thus, we can use Figure 8 to determine the asymmetry ratio for any grating: experimental sets of E_n (circles) and O_n (squares) are matched to the theoretical curves in the Figure and the asymmetry ratio is given by the data's resultant placement on the x-axis. For example, a Au nanowire grating that exhibited a total of four minima in its diffraction data ($E_1 = 12$, $O_1 = 25$, $E_2 = 36$, $O_2 = 49$) is best fit to the theoretical curves in Figure 8 at an asymmetry ratio of 8.2%. The diffraction data and asymmetry ratios for a total of 9 different nanowire arrays (6 Au and 3 Pd) are shown in the Figure. Each set of minima from a particular nanowire array are linked with a vertical dash-dotted line.

We have used this methodology to determine the asymmetry for over 20 different nanowire arrays. SEM measurements were also taken for a subset of these arrays; for all of these cases, the average value of $\%\Delta/d$ obtained from the diffraction data matched that obtained from SEM measurements. Small variations were observed from spot to spot on a given grating – we attribute those variations to small true local variations in $\%\Delta/d$ caused by imperfections in the LPNE process.

ER and TIR Nanowire Array Diffraction Measurements

All of the diffraction data shown in Figure 8 are from diffraction patterns obtained in the transmission geometry (Figure 3a). Diffraction data were also obtained from nanowire arrays in ER geometry (Figure 3b) and TIR geometry (Figure 3c). In both of these geometries, the HeNe laser is *p*-polarized with respect to the grating surface, and the angle of incidence is set to Brewster's angle θ_b, which for the air/BK-7 interface in the ER geometry is 56.6°, and for the BK-7/air interface in the TIR geometry is 33.4°. For diffraction measurements in a reflection geometry, the full grating equation is given by eq 7:

$$m\lambda = \eta D(\sin\theta_b + \sin\theta_m)$$

(7)

where η is the refractive index of the incident media ($\eta = 1.000$ for ER, $\eta = 1.515$ for TIR). Figure 9 shows a diffraction image and line profile obtained in the ER geometry from an array of gold nanowires with widths of 120 nm and an average spacing of 25 μm. There are three advantages for the ER geometry as compared to the transmission geometry:

i.   Since the laser is incident on the sample at Brewster's angle in the ER geometry, there is almost no specular ($m = 0$) reflection at $-\theta_b$. This results in a large reduction of background scattering that makes it possible to measure the diffraction intensities of the lower (*e.g.*, $m = 1, 2, 3$) orders. Measuring the intensity of these low orders was extremely difficult in the transmission geometry due to the high intensity of the $m = 0$ order spot.

ii. In the ER geometry it is possible to measure more diffraction orders as compared to the transmission geometry. This is because the HeNe laser incident angle is at 56.6°, which means that the available angle range to observe positive orders is 146.6°, as compared to just 90° for the transmission geometry. For a grating spacing D of 50 μm, the grating equation (eq 7) predicts that a maximum of 144 orders should be observable as compared to 78 orders for transmission geometry.

iii. As seen in Figure 9, the widths of the diffraction peaks on the detection screen are more regular for the ER geometry as compared to those obtained in the transmission geometry. This again is due to angle of incidence of the HeNe laser beam (See Figure 3b). Also seen in the ER data is a very small set of diffraction peak shoulders in the 400−800 pixel region due to diffraction by a small portion of the laser beam reflected at the second BK7/air interface.

One additional factor we have neglected to mention for both the ER and transmission geometries is the Fresnel reflection coefficient. In fact, it is this Fresnel coefficient that leads to the strong reduction in the $m = 0$ reflection for the ER geometry. In principle, all of the diffraction peak intensities include a Fresnel factor for the angle that each diffracted beam makes with the substrate surface. This becomes particularly important for diffraction measurements that employ a TIR geometry (Figure 3c).

Figure 10 shows the diffraction pattern obtained in the TIR geometry from an array of Pd nanowires with a width of 85 nm and an average spacing of 25 μm. The angle of incidence of the HeNe laser was Brewster's angle (33.4°). As in the case of the ER geometry, this incident angle was chosen to greatly reduce the reflected $m = 0$ diffraction order intensity. A significant enhancement is observed for diffraction orders $m > 13$, which have angles of reflection greater than the critical angle (41.3°). This enhancement factor leads to an increased sensitivity in the TIR geometry (~3−4x). This sensitivity enhancement permitted us to see very small nanowires in TIR geometry (both Au and Pd), down to 25 nm. The TIR diffraction measurements can be easily incorporated into biosensor formats that require an *in situ* flow cell.[28, 29] In future experiments, we will employ the TIR geometry for diffraction measurements from gratings in microfluidic flow channels.

Conclusions

In summary, we have described how simple optical diffraction measurements can be used to characterize micron scale arrays of both Au and Pd nanowires created by the electrochemical LPNE process. The intensity of the diffraction from the nanowire arrays depends on the square of the nanowire width *w*; diffraction was observed for nanowires with thicknesses down to 25 nm corresponding to 0.1% of the surface. The nanowire arrays yield unique diffraction data over many orders (>60) with separate oscillating intensity patterns for even and odd order intensities. These intensity patterns are attributed to the asymmetric alternate spacing ($d+\Delta$, $d-\Delta$) of the nanowires in the array that is a direct consequence of the LPNE process. Using a

simple FT analysis, a value for asymmetry Δ in the grating patterns can be obtained from the intensity patterns in the diffraction data. All of the diffraction measurements in this paper were obtained at a wavelength of 633 nm; future experiments will examine the wavelength dependence of the nanowire diffraction, including surface plasmon enhancements. In the future, we will also examine how changes in the diffraction patterns and intensity from nanowire arrays can be used to monitor the adsorption and desorption of molecules for sensing and biotechnology applications.

Acknowledgments

Appendix

Appendix

Mathematics of Asymmetric Grating Models

In this appendix, we describe a mathematical model for the nanowire arrays created by the electrochemical LPNE process, and then derive equations for (i) the oscillating intensities of the even and odd orders of the diffraction patterns observed from these nanowire arrays, and (ii) equations that describe the orders at which minima occur in the oscillating intensities of the even and odd orders.

To model the nanowire arrays, we first create an asymmetric grating unit cell, $h_1(x)$, that is composed of two square pulses of width w and height A, centered at $x = 0$ and $x = d-\Delta$ (Figure 7a).

$$h_1(x) = \begin{cases} 0 & x < -w/2 \\ A & -w/2 \leq x \leq w/2 \\ 0 & w/2 < x < d - \Delta - w/2 \\ A & d - \Delta - w/2 \leq x \leq d - \Delta + w/2 \\ 0 & x > d - \Delta + w/2 \end{cases}$$

(A.1)

By convoluting the asymmetric unit cell with an infinite array of delta functions (Dirac comb) of spacing $2d$, $h_2(x)$ (Figure 7b),

$$h_2(x) = \sum_{m=-\infty}^{\infty} \delta(x - 2dm)$$

(A.2)

the result is an infinite asymmetric array, $h_3(x)$, that serves as the model for the nanowire arrays:

$$h_3(x) = \int_{-\infty}^{\infty} h_1(x) h_2(x - \tau) \, d\tau = h_1(x) \otimes h_2(x) = \sum_{m=-\infty}^{\infty} h_1(x - 2dm)$$

(A.3)

This function is shown schematically in Figure 7c.

The diffraction pattern from the infinite asymmetric array can be obtained by taking the FT of the convolution in eq A.3. Rather than directly taking the FT[$h_3(x)$], we used the convolution theorem[30] and arrive at a simple analytical solution. First we need the FTs of $h_1(x)$ and $h_2(x)$, denoted as $H_1(u)$ and $H_2(u)$ respectively:

$$H_1(u) = Aw\left(1 + e^{-2\pi i(d-\Delta)u}\right)\operatorname{sinc}(\pi w u)$$

(A.4)

$$H_2(u) = \frac{1}{2d}\sum_{m=-\infty}^{\infty}\delta\left(u - \frac{m}{2d}\right)$$

(A.5)

where $\operatorname{sinc}(\pi w u) = \frac{\sin(\pi w u)}{\pi w u}$. The magnitude squared of $H_1(u)$ is plotted schematically in Figure 7d, and $H_2(u)$ is plotted schematically in Figure 7e.

The FT of $h_3(x)$, $H_3(u)$, can be obtained from the convolution theorem:

$$H_3(u) = \mathrm{FT}[h_3(x)] = \mathrm{FT}[h_1(x)\otimes h_2(x)] = H_1(u)H_2(u)$$

(A.6)

To obtain the diffraction peak intensity at a particular order $I(m)$, we integrate $|H_3(u)|^2$ around the peak with an infinitesimal displacement ε (to avoid having a multiplication by a delta function):

$$I(m) = \int_{\frac{m}{2d}-\varepsilon}^{\frac{m}{2d}+\varepsilon}|H_1(u)H_2(u)|^2 \mathrm{d}u = \left|\frac{1}{2d}H_1\left(\frac{m}{2d}\right)\right|^2 = \frac{A^2 w^2}{d^2}\cos^2\left[\frac{\pi}{2}\left(1-\frac{\Delta}{d}\right)m\right]\operatorname{sinc}^2\left(\frac{\pi}{2}\frac{w}{d}m\right)$$

(A.7)

This integration is essentially sampling the function $|H_1(u)|^2$ at values of $m/2d$ where m is an integer order number. The solution can predict the diffraction pattern of any asymmetric grating (or a symmetric grating if $\Delta = 0$).

The intensity for only even or only odd orders then becomes:

$$I_e(m) = \frac{A^2 w^2}{d^2}\cos^2\left(\frac{\pi}{2}\frac{\Delta}{d}m\right)\operatorname{sinc}^2\left(\frac{\pi}{2}\frac{w}{d}m\right)\qquad (m\quad\text{even})$$

(A.8)

$$I_o(m) = \frac{A^2 w^2}{d^2}\sin^2\left(\frac{\pi}{2}\frac{\Delta}{d}m\right)\operatorname{sinc}^2\left(\frac{\pi}{2}\frac{w}{d}m\right)\qquad (m\quad\text{odd})$$

(A.9)

These equations are used in Results and Discussion at eqs 3 and 4.

We can solve the $\cos^2$ and $\sin^2$ term for orders at which the minima occur for the even and odd order envelopes respectively:

$$m = \frac{d}{\Delta}(2n-1) = E_n\qquad (m\quad\text{even, and}\quad n=1,2,3)$$

(A.10)

$$m = \frac{d}{\Delta} 2n = O_n \qquad\qquad (\text{m \quad odd and} \quad n=1, 2, 3)$$

(A.11)

These equations are used in Results and Discussion at eqs 5 and 6.

References

1. Hu JT, Odom TW, Lieber CM. Acc. Chem. Res 1999;32:435–445.

2. Xia Y, Yang P, Sun Y, Wu Y, Mayers B, Gates B, Yin Y, Kim F, Yan H. Adv. Mater 2003;15:353–389.

3. Xiang CX, Yang YG, Penner RM. Chem. Commun 2009:859–873.

4. Favier F, Walter EC, Zach MP, Benter T, Penner RM. Science 2001;293:2227–2231. [PubMed: 11567132]

5. Murray BJ, Li Q, Newberg JT, Hemminger JC, Penner RM. Chem. Mater 2005;17:6611–6618.

6. Wan Q, Li QH, Chen YJ, Wang TH, He XL, Li JP, Lin CL. Appl. Phys. Lett 2004;84:3654–3656.

7. Yang F, Taggart DK, Penner RM. Nano Lett. 2009in press

8. Patolsky F, Zheng GF, Lieber CM. Nat. Protoc 2006;1:1711–1724. [PubMed: 17487154]

9. He B, Morrow TJ, Keating CD. Curr. Opin. Chem. Biol 2008;12:522–528. [PubMed: 18804551]

10. Cui Y, Wei QQ, Park HK, Lieber CM. Science 2001;293:1289–1292. [PubMed: 11509722]

11. Xiang C, Guell AG, Brown MA, Kim JY, Hemminger JC, Penner RM. Nano Lett 2008;8:3017–3022. [PubMed: 18712931]

12. Menke EJ, Thompson MA, Xiang CX, Yang LC, Penner RM. Nat. Mater 2006;5:914–919. [PubMed: 17057701]

13. Xiang CX, Kung SC, Taggart DK, Yang F, Thompson MA, Guell AG, Yang YA, Penner RM. ACS Nano 2008;2:1939–1949. [PubMed: 19206435]

14. Tsay YG, Lin CI, Lee J, Gustafson EK, Appelqvist R, Magginetti P, Norton R, Teng N, Charlton D. Clin. Chem 1991;37:1502–1505. [PubMed: 1893575]

15. St John PM, Davis R, Cady N, Czajka J, Batt CA, Craighead HG. Anal. Chem 1998;70:1108–1111. [PubMed: 9530002]

16. Nakajima F, Hirakawa Y, Kaneta T, Imasaka T. Anal. Chem 1999;71:2262–2265.

17. Morhard F, Pipper J, Dahint R, Grunze M. Sens. Actuators, B 2000;70:232–242.

18. Bailey RC, Hupp JT. J. Am. Chem. Soc 2002;124:6767–6774. [PubMed: 12047198]

19. Bailey RC, Nam JM, Mirkin CA, Hupp JT. J. Am. Chem. Soc 2003;125:13541–13547. [PubMed: 14583051]

20. Yu F, Tian SJ, Yao DF, Knoll W. Anal. Chem 2004;76:3530–3535. [PubMed: 15228321]

21. Goh JB, Loo RW, Goh MC. Sens. Actuators, B 2005;106:243–248.

22. Yu F, Knoll W. J. Nonlinear Opt. Phys. Mater 2005;14:149–160.

23. Bornhop DJ, Latham JC, Kussrow A, Markov DA, Jones RD, Sorensen HS. Science 2007;317:1732–1736. [PubMed: 17885132]

24. Wark AW, Lee HJ, Qavi AJ, Corn RM. Anal. Chem 2007;79:6697–6701. [PubMed: 17676761]

25. Sendroiu I, Corn RM. Biointerphases 2008;3:23–29.

26. Steward, EG. Fourier optics : an introduction. Vol. 2nd ed.. Ellis Horwood; Chichester: 1987.

27. Lexholm M, Hessman D, Samuelson L. Nano Lett 2006;6:862–865. [PubMed: 16608299]

28. Sarov Y, Ivanov T, Ivanova K, Sarova V, Capek I, Rangelow IW. Appl. Phys. A: Mater. Sci. Process 2006;84:191–196.

29. Loo RW, Tam PL, Goh JB, Goh MC. Anal. Biochem 2005;337:338–342. [PubMed: 15691515]

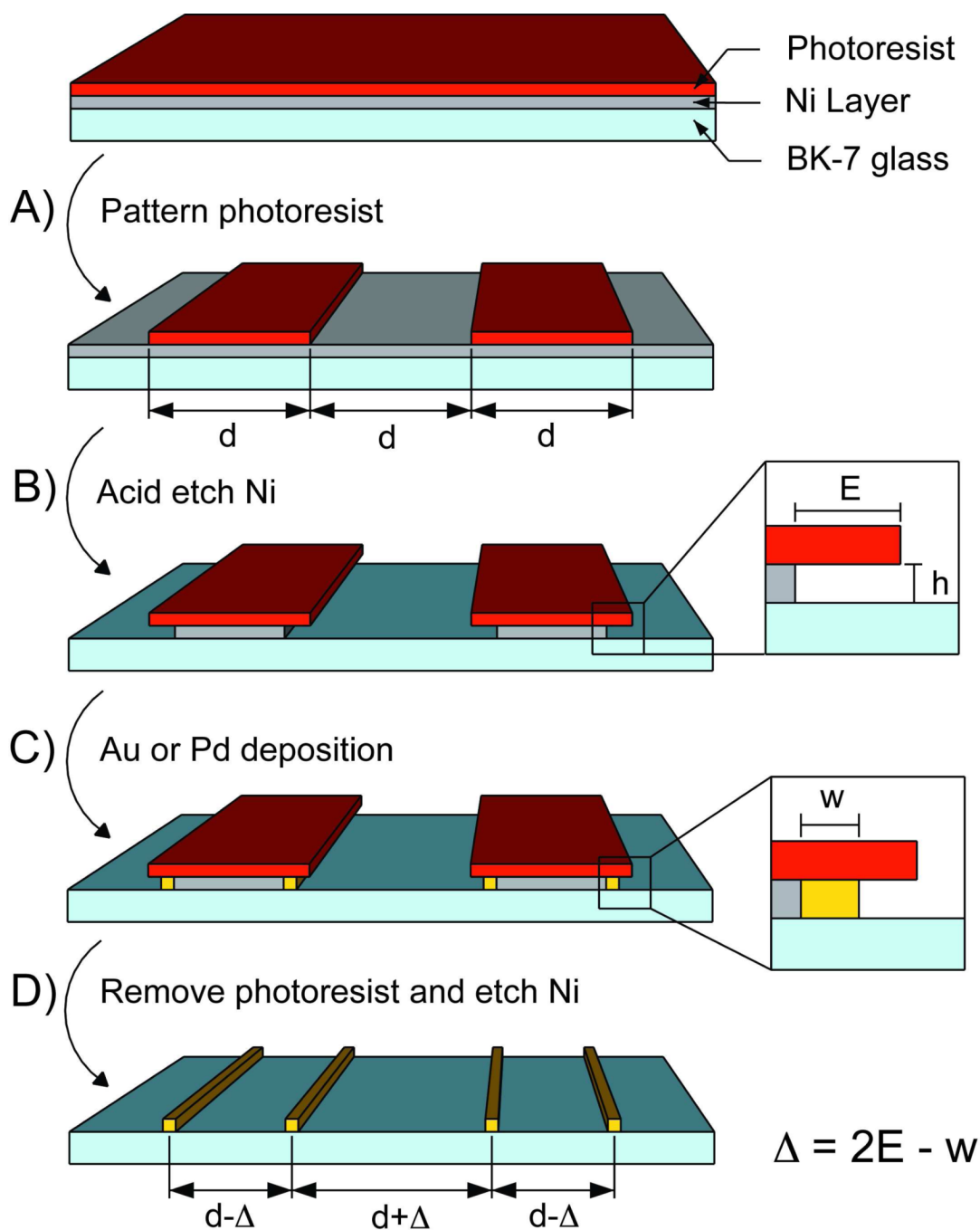30. Brigham, EO. The fast Fourier transform. Prentice-Hall; Englewood Cliffs, N.J.: 1974.

Figure 1.
Schematic flow diagram of the LPNE process for fabrication of either Au or Pd nanowire gratings with nanowire height h of 45 nm, width w of 25−150 nm and alternating inter-wire spacing $d-\Delta$ and $d+\Delta$ where d is 25 μm and Δ is a deviation from symmetry varying from 0 to 3.5 μm due to the asymmetric etching depth E, and growing as defined in the figure. See text for details.
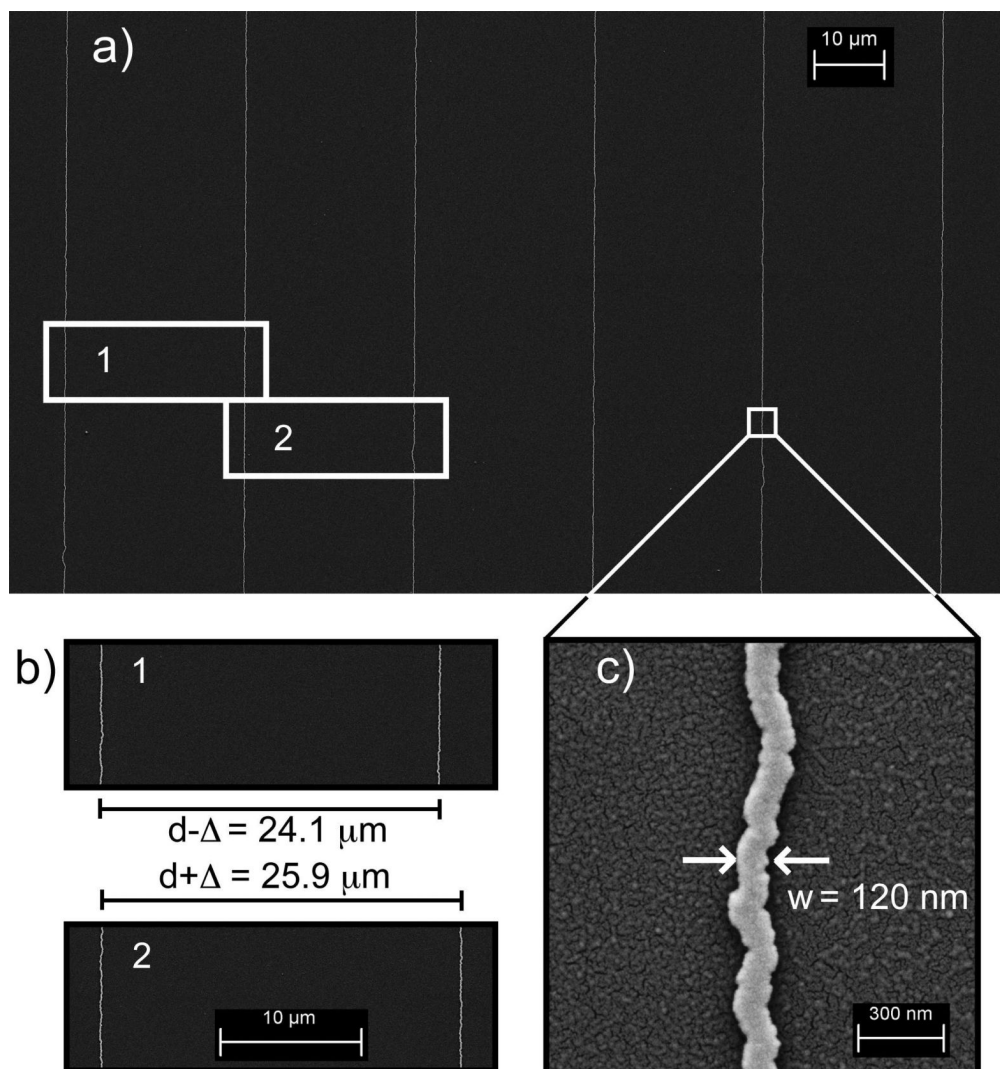
Figure 2.
SEM images of an Au nanowire grating: a) Large area scan showing average wire spacing of 25 μm. b) Overlaying images of a neighboring nanowire pair revealing asymmetry due to the etching and growing steps where $d-\Delta = 24.1$ μm, $d+\Delta = 25.9$ μm. c) High magnification image of a single Au nanowire with $w = 120$ nm.
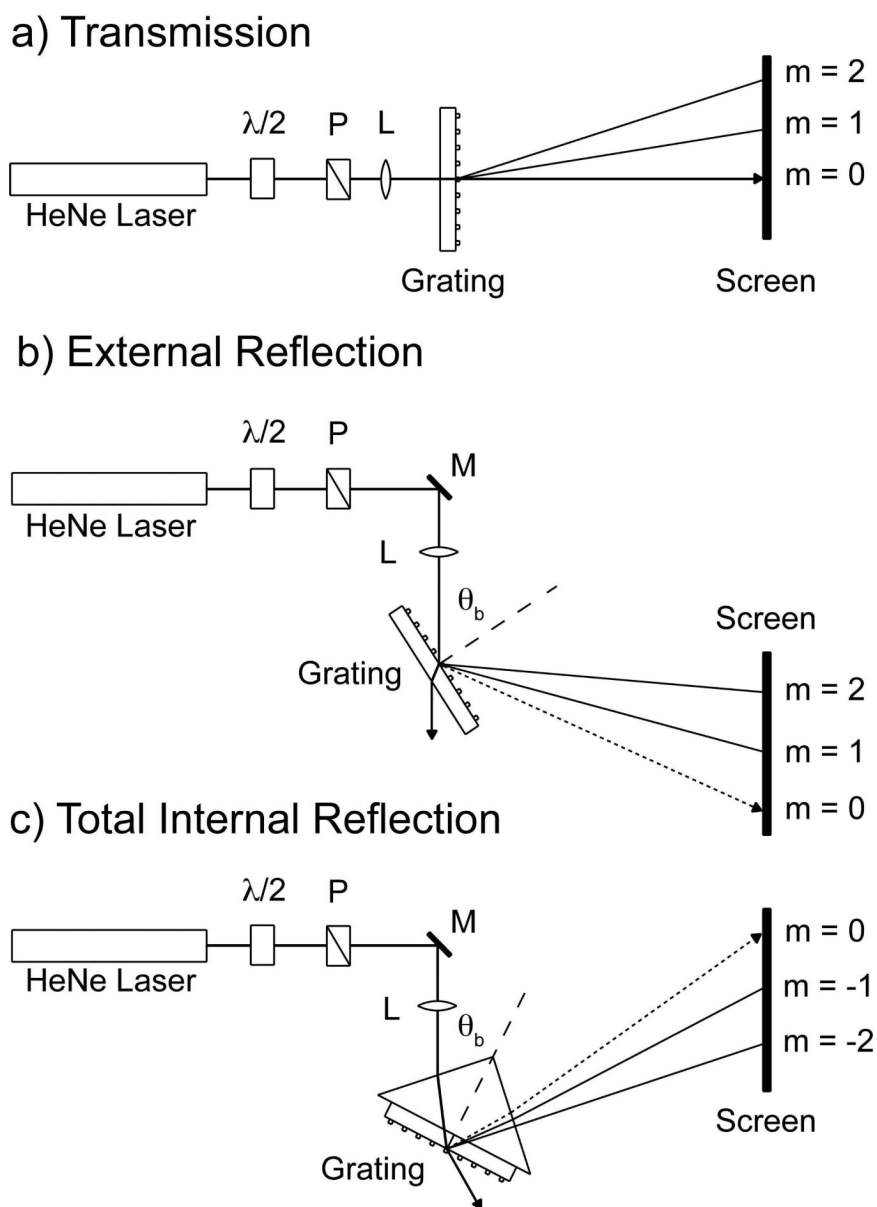
Figure 3.
Schematic diagram of the three geometries used to obtain diffraction images. In all cases the source is a HeNe laser with a polarizer (P) and a $\lambda/2$ plate to control the intensity and final polarization, and a lens (L) t20 focus the image on the screen. a) In Transmission geometry the laser impinges normal to the surface. b) In External reflection and c) Total internal reflection geometry the laser impinges at Brewster's angle (θ_b) for an air-glass and glass-air interface respectively.
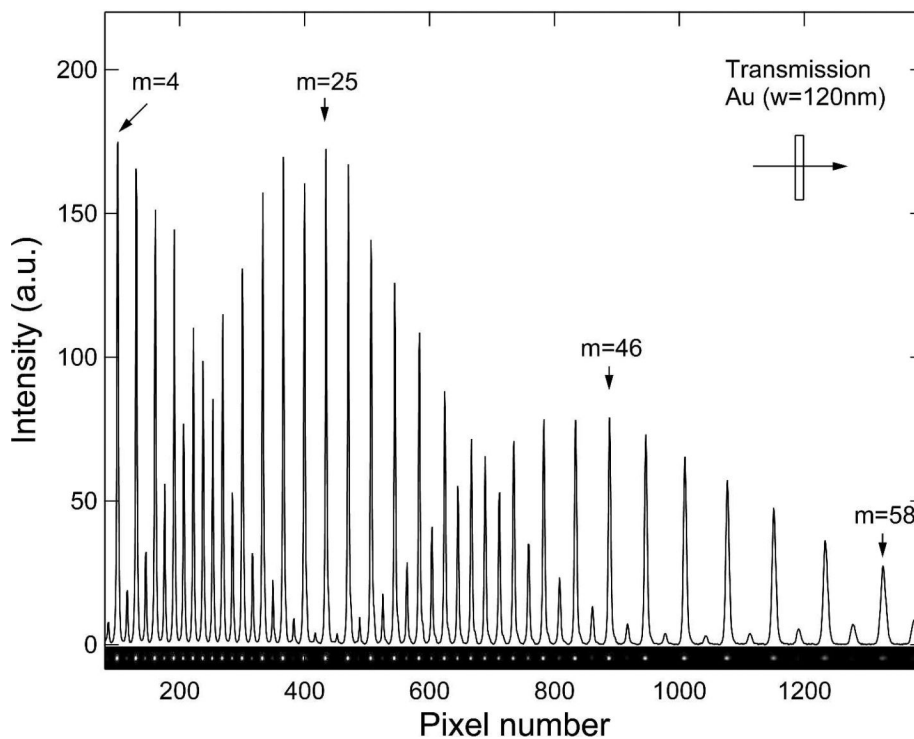
Figure 4.
Transmission geometry line profile of the diffraction pattern of an Au nanowire grating with w = 120 nm and Δ/d = 4.0%, displaying orders from m = 3 to 59. Beneath is the image used to obtain the line profile with enhanced contrast to easily visualize the diffraction spots.
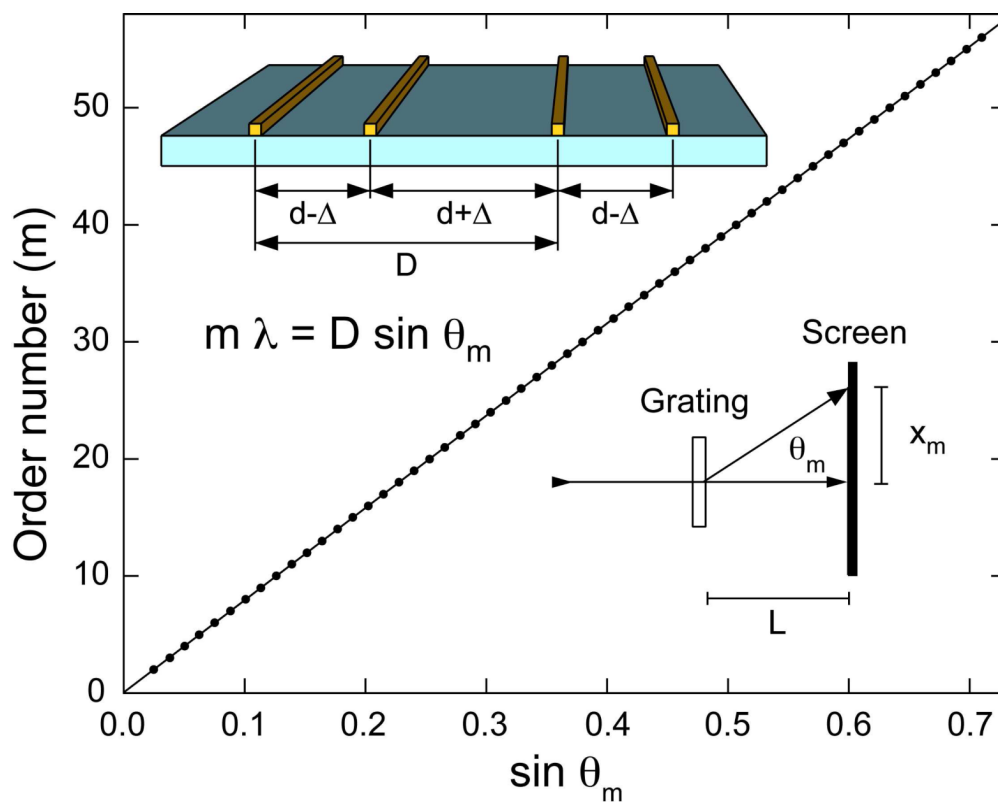
Figure 5.
Plot of experimentally determined order number (*m*) versus $\sin\theta_m$ as defined by the bottom inset where each dot represents one order. The solid line is the fit as predicted by the grating equation (eq 2). A zero intercept ensures the orders number were assigned correctly and the slope of the line is D/λ, where $D = 50.2 \pm 0.1$ μm. The top inset shows how the asymmetry forces the grating period $D = 2d$.
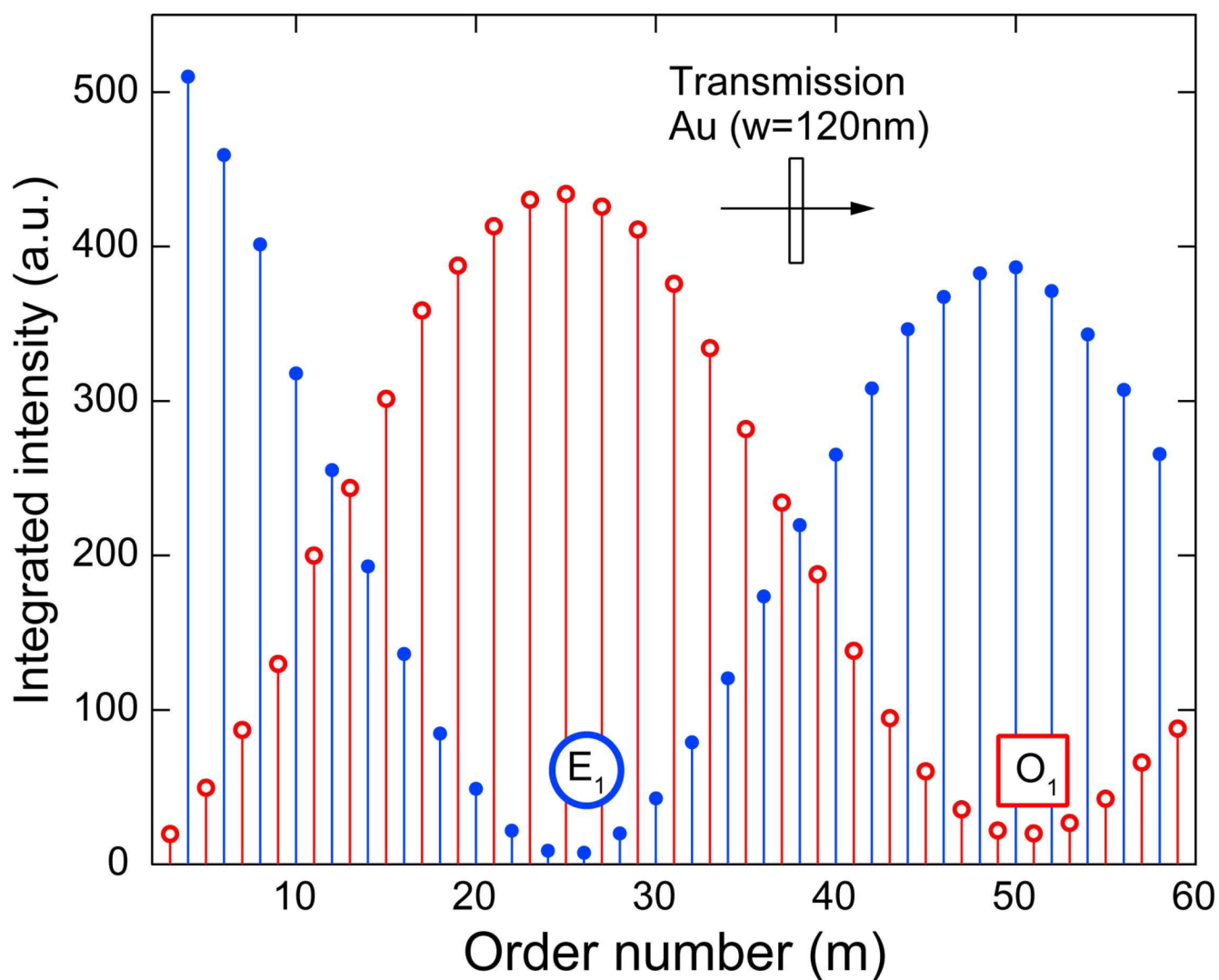
Figure 6.
Integrated diffraction spot intensities from the line profile in Figure 4 plotted versus order number where blue solid dots are the even orders and red open dots are the odd orders. The order of first minimum for the even order peaks is denoted E_1 (circle) and the order of first minimum for the odd order peaks is denoted O_1 (square).
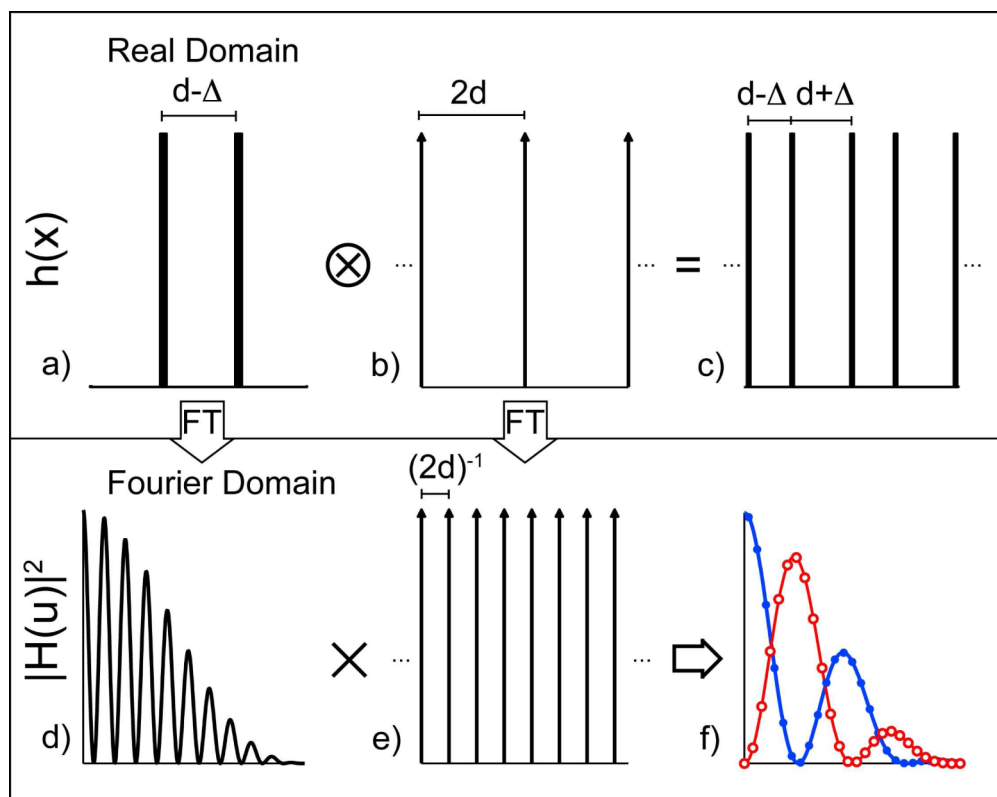
Figure 7.
Schematic diagram of the convolution theorem analysis involved in finding the diffraction pattern of a particular grating. The grating is modeled in the real domain: a) an asymmetric grating unit cell formed by two square pulses is convoluted with b) a Dirac comb of spacing 2d to yield c) an infinite asymmetric grating. The diffraction pattern is found in the Fourier domain: d) The FT of the unit cell (plotted as the $|FT|^2$) is multiplied by e) the FT of the Dirac comb. The square magnitude of each integrated peak is taken to yield f) the predicted diffraction pattern, where the solid blue dots are the even orders and open red dots are the odd orders. The solid lines in Figure 7f are the intensity functions for the even and odd orders (see eqs 3 and 4).
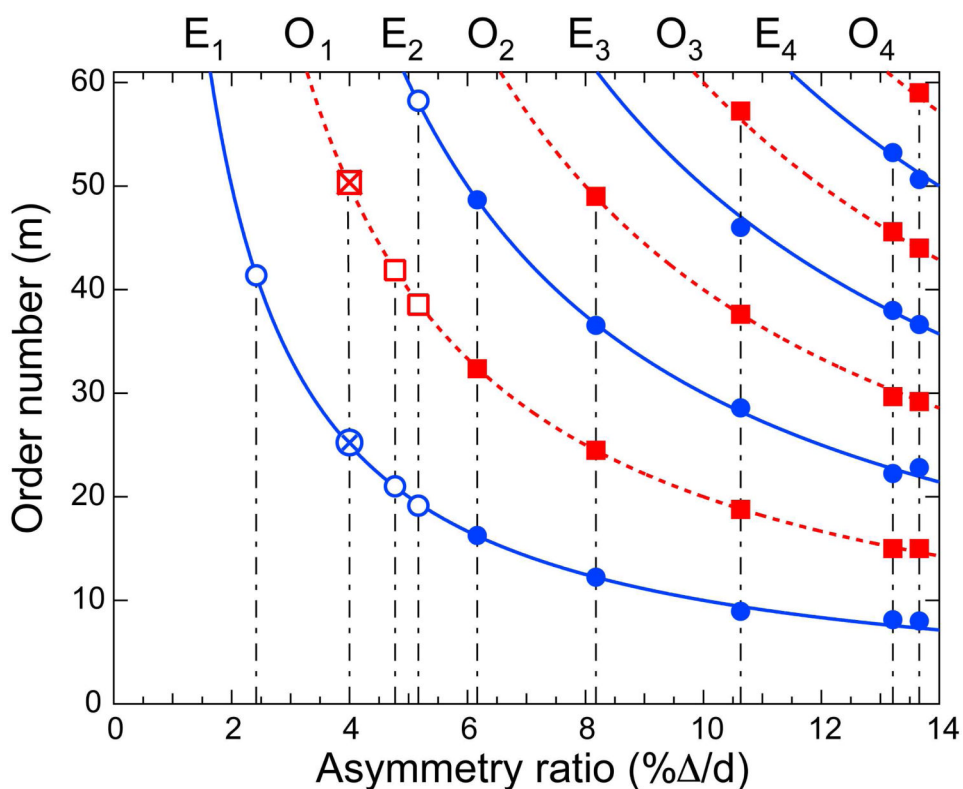
Figure 8.
Plot of the order of occurrence of even (E_n, solid curves) and odd (O_n, dashed curves) minima versus the percent asymmetry ratio as predicted by eqs 5 and 6. Vertical dash-dotted lines represent each sample with circles as their even minima and squares as their odd minima. 6 Au (solid) and 3 Pd (open) grating diffraction patterns are fit to the curves to determine their asymmetry ratio, Δ/d. The Au sample from Figure 6 is depicted by the open-crossed symbols at $\Delta/d = 4.0\%$.
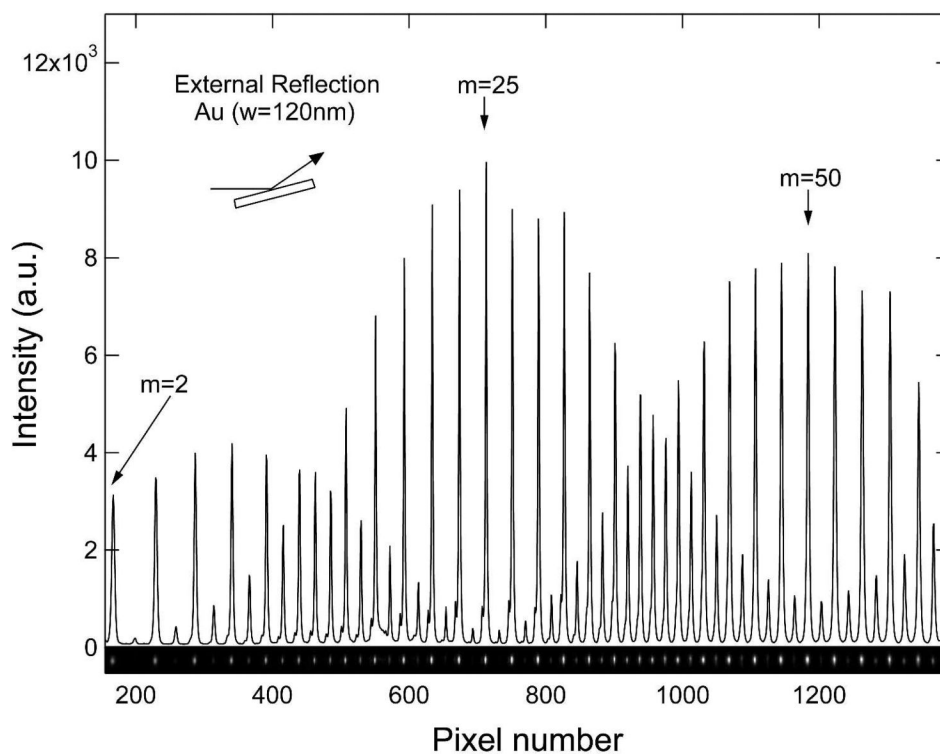
Figure 9.
External reflection geometry line profile of the diffraction pattern of an Au nanowire grating with w = 120 nm and Δ/d = 4.0%. Beneath is the image used to obtain the line profile with enhanced contrast to easily visualize the diffraction spots.
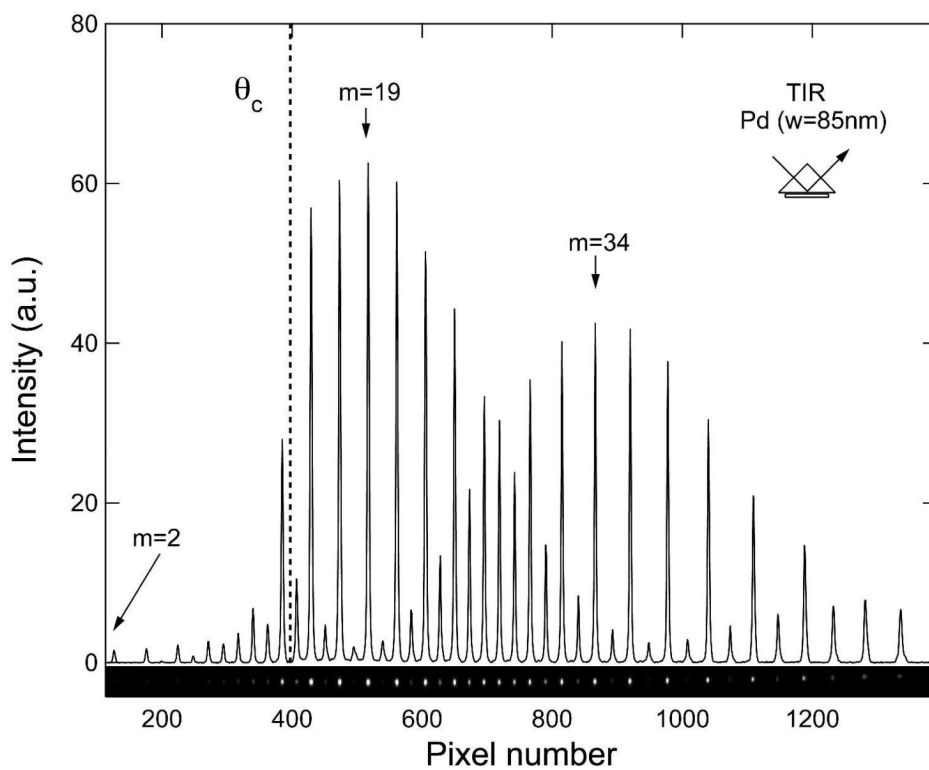
Figure 10.
Total internal reflection geometry line profile of the diffraction pattern of a Pd nanowire grating with $w = 85$ nm and $\Delta/d = 5.2\%$. The critical angle is marked, θ_c with the vertical dashed line after $m = 13$ for a glass-air interface. Beneath is the image used to obtain the line profile with enhanced contrast to easily visualize the diffraction spots.